ARCHIVES OF ELECTRICAL ENGINEERING VOL. 67(3), pp. 485–497 (2018)

DOI 10.24425/123658

A hybrid active fault-tolerant control scheme for wind energy conversion system based on permanent magnet synchronous generator

AHMED TAHRI[1], SAID HASSAINE[1], SANDRINE MOREAU[2]

[1] *Laboratoire de Génie Energétique et Génie Informatique L2GEGI*
Université Ibn Khaldoun de Tiaret, Tiaret, Algérie

[2] *Laboratoire d'Informatique et d'Automatique pour les Systèmes LIAS*
Université de Poitiers, Poitiers, France
e-mail: ahmed.tahri@univ-tiaret.dz, s_hassaine@yahoo.fr, sandrine.moreau@univ-poitiers.fr

(Received: 30.12.2017, revised: 23.04.2018)

Abstract: Wind energy has achieved prominence in renewable energy production. Therefore, it is necessary to develop a diagnosis system and fault-tolerant control to protect the system and to prevent unscheduled shutdowns. The presented study aims to provide an experimental analysis of a speed sensor fault by hybrid active fault-tolerant control (AFTC) for a wind energy conversion system (WECS) based on a permanent magnet synchronous generator (PMSG). The hybrid AFTC switches between a traditional controller based on proportional integral (PI) controllers under normal conditions and a robust *backstepping* controller system without a speed sensor to avoid any deterioration caused by the sensor fault. A sliding mode observer is used to estimate the PMSG rotor position. The proposed controller architecture can be designed for performance and robustness separately. Finally, the proposed method was successfully tested in an experimental set up using a *dSPACE 1104* platform. In this experimental system, the wind turbine with a generator connection via a mechanical gear is emulated by a PMSM engine with controled speed through a voltage inverter. The obtained experimental results show clearly that the proposed method is able to guarantee service production continuity for the WECS in adequate transition.

Key words: wind energy conversion system, active fault-tolerant control, permanent magnet synchronous generator, sensor fault diagnosis, sliding mode observer

1. Introduction

The petroleum crisis and the increasing demand for energy, combined with the possibility to reduce the supply of conventional fuels, have motivated progress in renewable energy research and applications. Among renewable energy sources, wind energy is currently considered to be the most useful natural energy source because it is abundant and clean [1]. Despite these advantages, the efficiency of wind energy conversion is currently low, and the initial cost for

its implementation is still considered high [2]. Therefore, the wind energy cost reduction is essential for the rapid spread of the wind power generation through a more efficient, reliable and cost-effective WECS [3]. Hence, the WECSs based on a PMSG show promising technology because of their high efficiency and absence of an external excitation system [4–5]. Moreover, the condition monitoring of these systems is considered to be an effective tool in reducing operational and maintenance costs [6].

Wind turbine conversion systems are growing in size and complexity, and are made (increasingly) of modern electrical devices. However, WECSs are generally subject to occurrences of various faults [7–8]. A fault in the device or its power supply may cause a substantial risk, an interruption in electricity production, equipment damages and may degrade the service quality and systems reliability [6].

A fault is an abnormal condition, which can lead to deviation of voltages and currents from nominal values or states [9]. There are many types of faults in electrical devices. Some are faults of sensor devices. Since sensors are necessary to get feedback information in the wind energy conversion systems (WECS), it is necessary to find out solutions to ensure the system service continuity in cases of sensor faults. A key issue is to prevent local faults from developing into system failures that may cause safety hazards, temporary suspension in production and possible detrimental environmental impacts. This can be achieved by fault tolerance which means that faults are compensated in such a way to prevent system failures [10].

There are numerous study results about fault detection and fault-tolerant control, most focused on the faults of power semiconductors of inverters [11] and stator windings [12] of the motor drives. But few of them focused on speed/position sensor fault-tolerant control, especially for WECS application [13]. In [14] authors propose a fault detection and isolation (FDI) method for current and rotor position sensors in the PMSG of a WECS. However, fault tolerant control is not studied/addressed. In [15] the design of a fault-tolerant controller based on observers for a PMSM drive is proposed. Two-stage extended Kalman filter (EKF) and a back electromotive-force (EMF) adaptive observer (AO) are used to detect a position fault sensor. However, this method is complex.

This paper presents an experimental study of a simple and effective active fault-tolerant control scheme for WECS based-PMSG. The wind turbine with a generator connection via a mechanical gear is emulated by a PMSM engine with controlled speed through a voltage inverter. The proposed method can accurately detect mechanical sensor faults in real time and provides useful information about the detected faults. In addition, this method exploits only the input/output measurements which are available in the system without additional hardware complexity. The proposed method combines a traditional controller based on PI controllers, a robust *backstepping* control and a sliding mode observer for estimating rotor speed. The speed will be solely controlled by the PI controllers for a nominal model without disturbances [16–17]. However, in the presence of uncertainties or an external disturbance such as a fault, the *backstepping* robust controller will be activated and the measured velocity will be replaced by the speed calculated by the observer (sensorless control). This configuration improves system reliability and ensures availability of the WECS by an effective detection of speed sensor faults and a good transition between the controllers.

This paper is organized as follows: section 2 presents the control objectives of the system. The sensor fault detection and the control reconfiguration are detailed in section 3. In section 4,

the experimental results are presented. Finally an overall conclusion is presented at the end of the paper.

2. Control objectives

The first objective is to carry out a wind turbine emulator to simulate the behavior of a wind turbine with a PMSM. Indeed, the principle is the feedback control of the motor speed, in order to follow perfectly the reference speed Ω^* calculated by the wind turbine model as shown in Fig. 1, where G_r is the gearbox ratio [18]. The second objective is to ensure service continuity of the PMSG, while maintaining the performance and robustness of the PMSG by a hybrid speed sensor active fault-tolerant control (AFTC). The control algorithm is evaluated in a test bed as illustrated in Fig. 5.

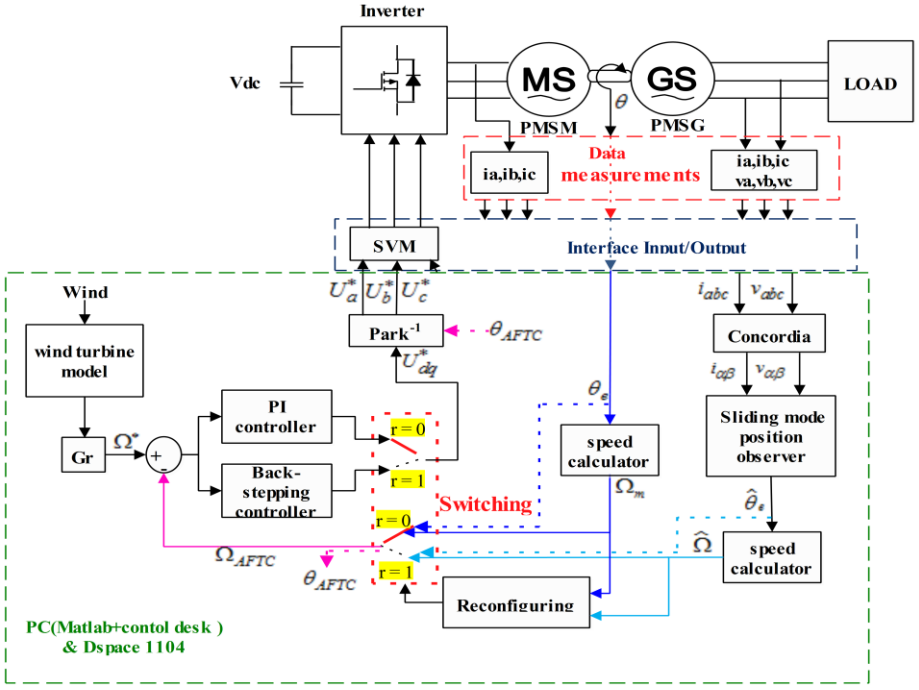

Fig. 1. Block diagram of the AFTC scheme

3. Active fault-tolerant control

3.1. Hybrid AFTC

In order to achieve system performance and robustness objectives of the wind turbine, we propose a hybrid controller by switching between two controllers, where the proposed controller

architecture can be designed for performance and robustness separately, which has the potential to overcome the conflict between performance and robustness in the traditional feedback framework. The controller is designed in such a way that the feedback speed control of the PMSG will be solely controlled by the PI controller performance for a nominal model without disturbances. The *backstepping* robust controller will only be activated in presence of uncertainties or an external disturbance, such as a fault.

The general active fault-tolerant control scheme to a speed-sensor fault is shown in Fig. 1. We use a PI controller in normal operation and a robust *backstepping* controller in the presence of the fault. This structure is one of the AFTC approaches. The AFTC principle can be divided into three steps: residual generation, fault detection and reconfiguration.

a. Residual generation

The residual signal r_y is the difference between the motor speed and the estimated speed given by the sliding mode observer as shows Fig. 2. Then the diagnosis scheme is designed to detect the fault occurrence from the residual value.

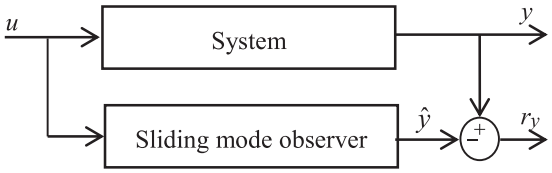

Fig. 2. Residual generation block diagram

b. Fault detection

When the speed sensor is affected by a bias fault, the residual is simply compared with a threshold to generate the binary control signal. The threshold is selected at 10 rad/s, which has been determined as a multiple of the standard deviation in normal operation [19]. However, when the measured speed delivered by the sensor is corrupted by noise, the residual is processed through the scheme shown in Fig. 3. The fault indicator (r) is set to 1 only when the residual is larger than the chosen threshold persistently over a certain period T_d (in this case T_d is chosen to be 0.1 s). This configuration eliminates any false alarm caused by the measurement noise. Unlike the persistent block used in [20], which is limited because it adds an additional heaviness to the computing device (*dSPACE*), we propose a simple persistent-block implemented in Matlab/Simulink as is shown in Fig. 4, where the persistence time delay is defined as the time response (T_d) of the transfer function.

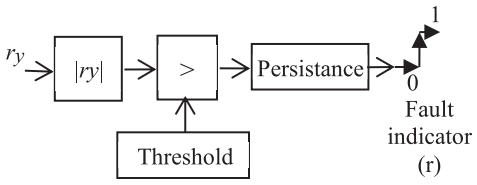

Fig. 3. Fault detection block diagram

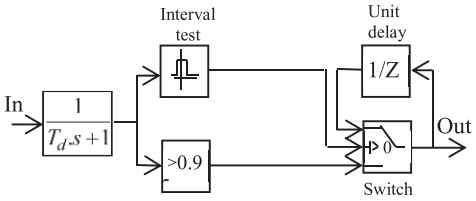

Fig. 4. Persistent block diagram

c. Reconfiguration

In normal operation, the PMSG feedback speed control is solely controlled by the PI controller performance. However, in the presence of the uncertainties or an external disturbance such as a fault, the reconfiguring block activates the switching from the normal operation to the robust *backstepping*-sensorless control. The *backstepping* controller and the sliding mode observer are designed in the following subsection.

3.2. Robust backstepping control

The *backstepping* technique is a systematic and recursive method for synthesizing nonlinear control laws. It uses the *Lyapunov* stability principle, which can be applied to a large number of nonlinear systems. The objective of the nonlinear *backstepping* controller is to track the PMSM speed with the appropriate choice of regulated variables. From [18] the control inputs have been chosen in the PMSM Park reference frame as:

$$u_d = K_1 L_d \varepsilon_d + L_d \frac{\mathrm{d}\, i_d^*}{\mathrm{d}\, t} + R_s i_d - \omega_e L_q i_q\,, \tag{1}$$

$$u_q = K_2 L_q \varepsilon_q + L_q \frac{\mathrm{d}\, i_q^*}{\mathrm{d}\, t} + R_s i_q + \omega_e (L_d i_d + \varphi_f), \tag{2}$$

where

$$\varepsilon_d = e_d + k_d \int_0^t e_d \,\mathrm{d}\, t, \qquad \varepsilon_q = e_q + k_q \int_0^t e_q \,\mathrm{d}\, t,$$

$$e_d = i_d^* - i_d\,, \qquad e_q = i_q^* - i_q$$

and K_1, K_2 are parameters introduced by the *backstepping* method.

They must always be positive and greater than k_d, k_q respectively, to attain the stability criteria of the *Lyapunov* function. Thus the virtual control is asymptotically stable. Besides, these parameters can influence the control dynamics; therefore, we must select them to ensure that the current dynamics converge faster than the speed ones. The superscript '*' denotes the reference signal.

3.3. Sliding mode observer

Unlike conventional observers design, the sliding mode observer for estimating rotor position angle uses only the electrical equations of the PMSG in the fixed coordinate (α, β) due to the fact that angular speed and position information are ready to be extracted in this reference frame [21]. The PMSG model in stationary (α, β) reference frame is:

$$\frac{\mathrm{d}\, i_\alpha}{\mathrm{d}\, t} = -\frac{R_s}{L_s} i_\alpha - \frac{1}{L_s} e_\alpha + \frac{u_\alpha}{L_s}, \tag{3}$$

$$\frac{\mathrm{d}\, i_\beta}{\mathrm{d}\, t} = -\frac{R_s}{L_s} i_\beta - \frac{1}{L_s} e_\beta + \frac{u_\beta}{L_s}, \tag{4}$$

$$e_\alpha = -\varphi_f \omega_e \sin(\theta_e), \tag{5}$$

$$e_\beta = \varphi_f \omega_e \cos(\theta_e). \tag{6}$$

The variables (i_α, i_β and u_α, u_β) in the fixed coordinate frame (α, β) are obtained by the Concordia transformation applied to measured three-phase electrical quantities (i_a, i_b, i_c and u_a, u_b, u_c) of the PMSG as shown in Fig. 1. θ_e is the electrical rotor position of the PMSG and L_s is its stator inductance where $L_s = L_\alpha = L_\beta$ (because the studied PMSG has nearly smooth poles).

Equations (3) and (4) can be expressed in matrix form as follows:

$$\dot{\boldsymbol{i}}_{\alpha\beta} = \boldsymbol{A}\,\boldsymbol{i}_{\alpha\beta} + \boldsymbol{B}(\boldsymbol{u}_{\alpha\beta} - \boldsymbol{e}_{\alpha\beta}), \tag{7}$$

where

$$\boldsymbol{A} = \begin{bmatrix} -\dfrac{R_s}{L_s} & 0 \\ 0 & -\dfrac{R_s}{L_s} \end{bmatrix}, \qquad \boldsymbol{B} = \begin{bmatrix} \dfrac{1}{L_s} & 0 \\ 0 & \dfrac{1}{L_s} \end{bmatrix},$$

$$\boldsymbol{i}_{\alpha\beta} = \begin{bmatrix} i_\alpha \\ i_\beta \end{bmatrix}, \qquad \boldsymbol{u}_{\alpha\beta} = \begin{bmatrix} u_\alpha \\ u_\beta \end{bmatrix}, \qquad \boldsymbol{e}_{\alpha\beta} = \begin{bmatrix} e_\alpha \\ e_\beta \end{bmatrix}.$$

The sliding mode observer (SMO) is designed in the following form:

$$\dot{\hat{\boldsymbol{i}}}_{\alpha\beta} = \boldsymbol{A}\hat{\boldsymbol{i}}_{\alpha\beta} + \boldsymbol{B}(\boldsymbol{u}_{\alpha\beta} + l\boldsymbol{Z}_{eq} + \boldsymbol{Z}), \tag{8}$$

where:

$$\boldsymbol{Z} = \begin{bmatrix} Z_\alpha \\ Z_\beta \end{bmatrix} = \begin{bmatrix} -K\,\mathrm{sign}\,(\hat{i}_\alpha - i_\alpha) \\ -K\,\mathrm{sign}\,(\hat{i}_\beta - i_\beta) \end{bmatrix}.$$

In (8) $\boldsymbol{Z}_{eq}$ represents the equivalent control and $\boldsymbol{Z}$ represents the discontinuous control, l is the feedback gain of the equivalent control, and K, generally positive ($K > 0$), is the switching gain of the discontinuous control. The hat $\hat{}$ indicates the estimated variable. The state model of the equivalent control ($\boldsymbol{Z}_{eq}$), after filtering the components of the discontinuous control $\boldsymbol{Z}$ by a low-pass filter (LPF), is given by the following expression:

$$\dot{\boldsymbol{Z}}_{eq} = \begin{bmatrix} \dot{Z}_{eq\alpha} \\ \dot{Z}_{eq\beta} \end{bmatrix} = \begin{bmatrix} -\omega_c Z_{eq\alpha} + \omega_c Z_\alpha \\ -\omega_c Z_{eq\beta} + \omega_c Z_\beta \end{bmatrix}. \tag{9}$$

It is noticed that its cutoff frequency ω_c must be properly designed with respect to the fundamental frequency of the PMSG currents.

The sliding surface is selected as $\boldsymbol{S} = 0$, where:

$$\boldsymbol{S} = \hat{\boldsymbol{i}}_{\alpha\beta} - \boldsymbol{i}_{\alpha\beta}\,.$$

By subtracting Equations (8) and (7) we can obtain the dynamic sliding mode motion equation as:

$$\dot{\boldsymbol{S}} = \boldsymbol{A}\,.\,\boldsymbol{S} + \boldsymbol{B}(\boldsymbol{e}_{\alpha\beta} + l\boldsymbol{Z}_{eq} + \boldsymbol{Z}). \tag{10}$$

If the switching gain K is large enough to ensure the following condition:

$$\dot{\boldsymbol{S}}^{\mathrm{T}}.\,\boldsymbol{S} < 0, \tag{11}$$

then the sliding mode occurs and we get $\boldsymbol{S} = 0$ which implies:

$$\boldsymbol{e}_{\alpha\beta} = \begin{bmatrix} e_\alpha \\ e_\beta \end{bmatrix} = -(1+l)\boldsymbol{Z}_{eq}\,. \tag{12}$$

The feedback gain l must be larger than -1 with any positive switching gain K, i.e. $l > -1$, which is the limit of the feedback gain of the equivalent control [21].

From (5) and (6), the angular rotor position θ_e can be estimated using the equivalent control $\boldsymbol{Z}_{eq}$ as:

$$\hat{\theta}_e = -\tan^{-1}\left(\frac{e_\alpha}{e_\beta}\right) = -\tan^{-1}\left(\frac{Z_{eq\alpha}}{Z_{eq\beta}}\right). \tag{13}$$

After that, the rotor speed is calculated from the estimation of the rotor position using a numerical derivation.

4. Experimental validation

In order to validate the developed method, a test bed has been set up. The used test bed consists of a PMSG driven by an actuator composed of a PMSM, power inverter and control. This set simulates a real wind turbine, by controlling the torque on the shaft and driving the PMSG, which delivers the produced energy on a resistive load. A *dSPACE DS1104 DSP* system is used to carry out the real-time algorithm. The used PMSM and PMSG are typically identical. The parameters are presented in Table 1. The configuration of the experimental test bed is shown in Fig. 5.

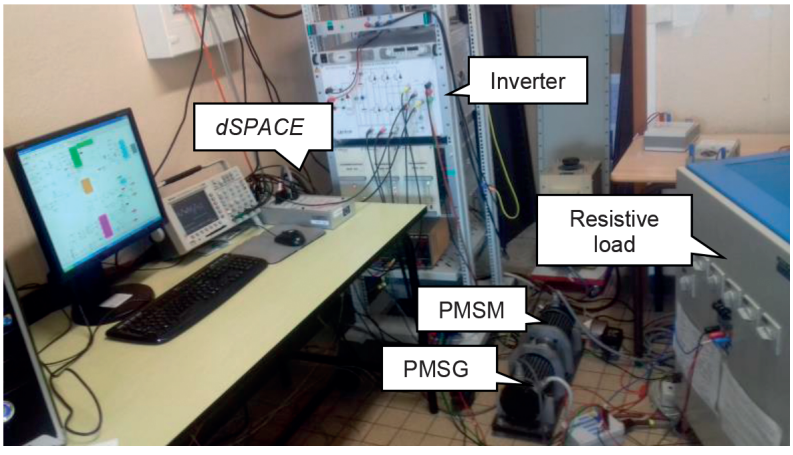

Fig. 5. WECS emulator: experimental setup

Table 1. PMSM parameters

Parameter name	Symbol	Value	Unit
Rated power	P	1	kW
Rated voltage	V	230	V
Rated line current	I	7	A
Rated rotational speed	n	1500	rpm
Stator inductance	L	4	mH
Stator resistance	R_s	0.57	Ω
Number of pole pairs	p	2	
Permanent magnet flux	φ_f	0.064	Wb
Viscous friction coefficient	B_m	0.0039	Nm/rad/s
Inertia moment	J_{eq}	0.00208	kg.m^2

The used position sensor is a resolver; it is subjected to three types of faults which are: exponential fault, offset fault and total resolver winding failure.

4.1. Exponential fault

In this experiment, the fault type is an exponential fault, which emulates a progressive bias on the speed measurement following the model given below:

$$\Omega_m = \begin{cases} \Omega & t < t_{\text{on}} \\ \Omega\left(1 - \frac{1}{3}\left(1 - e^{(-15(t-t_{\text{on}}))}\right)\right) & t > t_{\text{on}} \end{cases}, \tag{14}$$

where t_{on} is the activation time of the fault, Ω_m is the angular velocity measured by the sensor, and Ω is its real value.

The PMSG speed response is shown in Fig. 6(a) where it illustrates the measured speed Ω_m, the observed speed $\hat{\Omega}$, and the reconfiguration output speed Ω_{AFTC}.

Before the occurrence of the fault, the residue is about 0 as shown in Fig. 6(c). However, at $t = 3$ s, the residual increases gradually and exceeds the threshold value allowed at $t = 4.8$ s. Then, after a persistence time delay (about 0.1 seconds), the fault indicator signal varies from 0 to 1 as shown in Fig. 6(b). The latter activates the switching between the control with the speed sensor and without sensor. Figs. 6(d) and (e) show that the direct and the quadrature current responses of the PMSM are well controlled during the transition between the PI controllers and the non linear *backstepping* one. Finally, the three-phase current of the PMSG is shown in Fig. 6(f) where it is not affected before and after the reconfiguration.

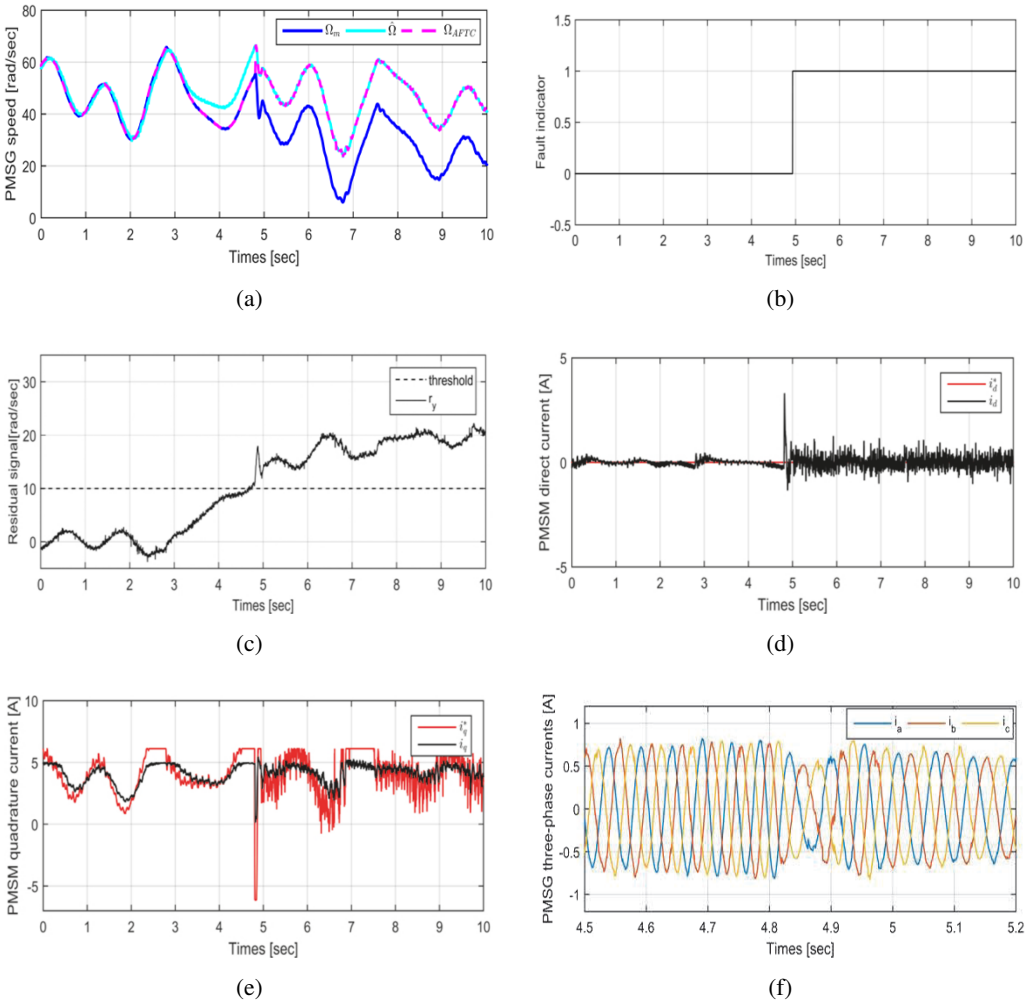

(a) (b) (c) (d) (e) (f)

Fig. 6. System performance under position sensor fault (exponential fault): (a) PMSG speed; (b) fault indicator; (c) residual signal; (d) direct current; (e) quadrature current; (f) three-phase currents

4.2. Offset fault

The sensor offset fault is a constant fault. It is modelled by a constant signal added to the measured speed. The Fig. 7 shows the evaluation of the speed control system under a constant fault which is applied at 4.85 s, where Ω_m is the measured speed, $\hat{\Omega}$ is the observed speed and Ω_{AFTC} is the reconfiguration output speed which is used by the control loop.

In normal operation, the residual signal is always lower than the threshold as shown in Fig. 7(c). However, when the residual exceeds the threshold value, the fault is detected and the binary control signal varies from 0 to 1 after the persistence time delay (at 4.95 s exactly) as shown in Fig. 7(b), which activates the switching between the PI controller (with speed sensor)

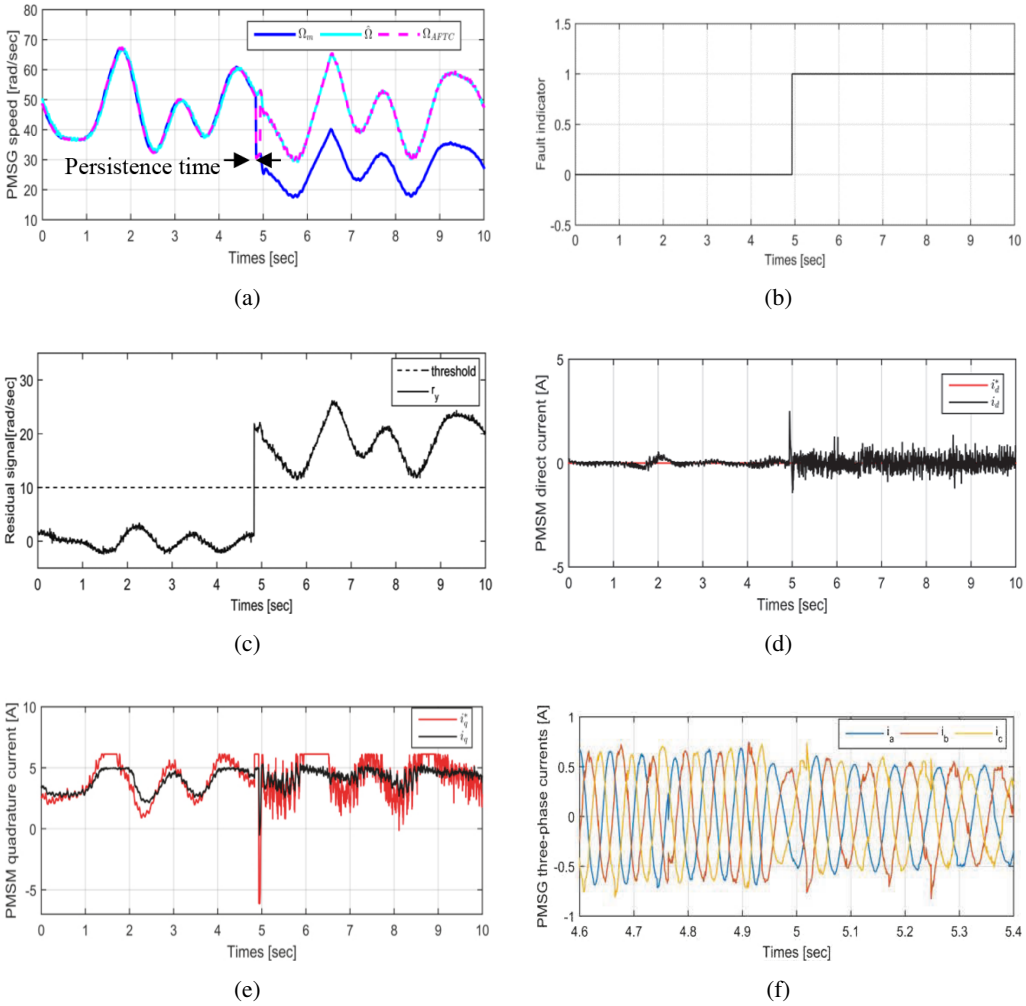

Fig. 7. System performance under position sensor fault (offset fault): (a) PMSG speed; (b) fault indicator; (c) residual signal; (d) direct current; (e) quadrature current; (f) three-phase currents

and the robust *backstepping*-sensorless control. Figs. 7(d) and (e) show the response of the direct and the quadrature PMSM currents, which are well controlled during the transition between the PI controller and the *backstepping* one. Finally, the three-phase currents of the PMSG are shown in Fig. 7(f), where they are not affected before and after the reconfiguration.

4.3. Total resolver winding failure

In this experiment, the mechanical sensor undergoes total failure. Before the fault occurrence, the residual is approximately 0, as shown in Fig. 8(a), where Ω_m, $\hat{\Omega}$ and Ω_{AFTC} are respectively

the measured speed, the observed speed and the speed used by the controllers. In normal operation, the residual signal is always lower than the threshold as shown in Fig. 8(c). However, the speed sensor fault occurs at 4.8 s, where the residual exceeds the threshold value, the binary control signal varies from 0 to 1 as shown in Fig. 8(b), which activates the switching between the PI controller and the robust *backstepping*-sensorless control ($\Omega_{AFTC} = \hat{\Omega}$). Figs. 8(d) and (e) show the response of the direct and the quadrature PMSM currents, which are well controlled during the transition between the PI controller and the *backstepping* one. Finally, the three-phase currents of the PMSG are shown in Fig. 8(f), where they are not affected before and after the reconfiguration.

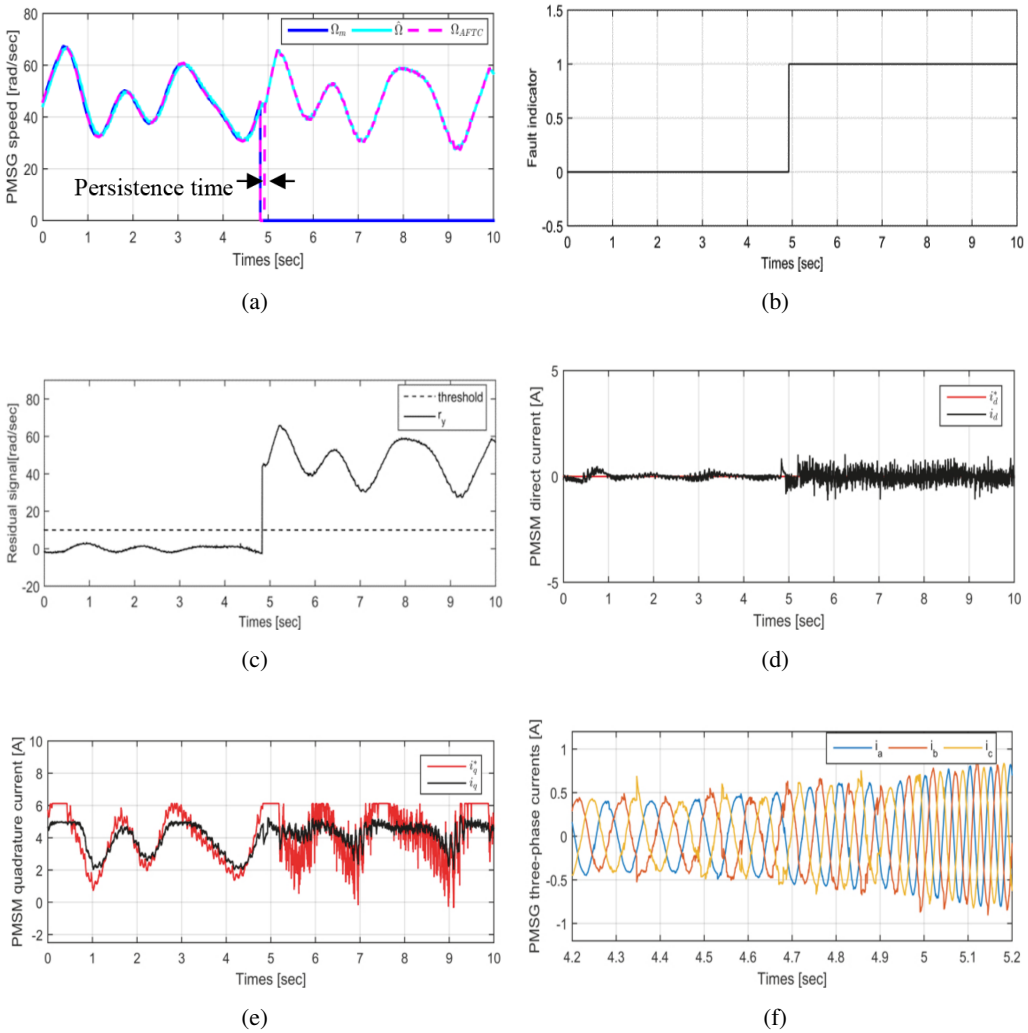

Fig. 8. System performance under position sensor fault (constant fault): (a) PMSG speed; (b) fault indicator; (c) residual signal; (d) direct current; (e) quadrature current; (f) three-phase currents

5. Conclusions

In this paper, a position sensor fault has been studied and a diagnostic procedure has been proposed and validated to improve the reliability and efficiency of the wind energy conversion system and to guarantee service continuity under different position sensor faults. The control is based on a hybrid of two controllers: a PI controller and a robust *backstepping* controller associated with a nonlinear sliding mode observer. The proposed hybrid AFTC is able to guarantee service production continuity for the WECS in good transition performance in presence of any speed sensor fault (total resolver winding failure, constant fault, and an exponential fault), and under variable velocity condition as in a real wind turbine situation. The proposed method has been tested successfully in real-time using *dSPACE 1104* platform. The obtained experimental results confirm the accuracy and the efficiency of the proposed method. Finally, as a further improvement of the WECS efficiency and reliability, it will be interesting to combine the proposed AFTC with a diagnostic procedure of phase current sensor fault.

Acknowledgements

This work has been supported by the Algerian government (PNE scholarship), and the Computer Science and Automatic Control for Systems Laboratory (LIAS laboratory) at the University of Poitiers, France.

References

[1] Ackermann T., *Wind power in power systems*, Wiley Online Library (2005).

[2] Walford C.A., *Wind turbine reliability: understanding and minimizing wind turbine operation and maintenance costs*, United States, Department of Energy (2006).

[3] Freire N.M.A., Estima J.O., Cardoso A.J.M., *A new approach for current sensor fault diagnosis in PMSG drives for wind energy conversion systems*, Proceedings of IEEE Energy Conversion Congress and Exposition, Raleigh, NC, USA, pp. 2083–2090 (2012).

[4] Hassaine S., Moreau S., Bensmaine F., *Design and hardware implementation of PMSM sliding mode control in SISO and MIMO cases*, Proceedings of IEEE 23rd International Symposium on Industrial Electronics (ISIE), Istanbul, Turkey, pp. 762–767 (2014).

[5] Gajewski P., Pieńkowski K., *Advanced control of direct-driven PMSG generator in wind turbine system*, Archives of Electrical Engineering, vol. 65, no. 4, pp. 643–656 (2016).

[6] Cheng M., Zhu Y., *The state of the art of wind energy conversion systems and technologies: A review*, Energy Conversion and Management, vol. 88, pp. 332–347 (2014).

[7] Talebi N., Sadrnia M.A., Darabi A., *Dynamic response of wind energy conversion systems under various faults*, International Journal of Engineering Systems Modelling and Simulation, vol. 7, no. 2, pp. 80–94 (2015).

[8] Kim Y.-M., *Data–driven modelling, control, and fault detection of wind turbine systems*, International Journal of System Control and Information Processing, vol. 1, no. 3, pp. 298–318 (2014).

[9] Byington C.S., Watson M., Edwards D., Stoelting P., *A model-based approach to prognostics and health management for flight control actuators*, Proceedings of IEEE Aerospace Conference, Big Sky, MT, USA, pp. 3551–3562 (2004).

[10] Fourlas G.K., *An approach towards fault tolerant of model-based hybrid control systems*, International Journal of Applied Systemic Studies, vol. 5, no. 3, pp. 199–214 (2014).

[11] Sobański P., Orłowska-Kowalska T., *Detection of single and multiple IGBTs open-circuit faults in a field-oriented controlled induction motor drive*, Archives of Electrical Engineering, vol. 66, no. 1, pp. 89–104 (2017).

[12] Toumi D., Boucherit M., Tadjine M., *Observer-based fault diagnosis and field oriented fault tolerant control of induction motor with stator inter-turn fault*, Archives of Electrical Engineering, vol. 61, no. 2, pp. 165–188 (2012).

[13] Bourogaoui M., Sethom H.B.A., Belkhodja I.S., *Speed/position sensor fault tolerant control in adjustable speed drives – A review*, ISA Transaction, vol. 64, pp. 269–284 (2016).

[14] Li H., Qu L., Qiao W., Wei C., *Current and rotor position sensor fault detection and isolation for permanent magnet synchronous generators in wind applications*, In IEEE Applied Power Electronics Conference and Exposition (APEC), Tampa, FL, USA, pp. 2810–2815 (2017).

[15] Akrad A., Hilairet M., Diallo D., *Design of a Fault-Tolerant Controller Based on Observers for a PMSM Drive*, IEEE Transactions on Industrial Electronics, vol. 58, no. 4, pp. 1416–1427 (2011).

[16] Tripathi S.M., Tiwari A.N., Singh D., *Controller Design for a Variable-Speed Direct-Drive Permanent Magnet Synchronous Generator-Based Grid-Interfaced Wind Energy Conversion System Using D-Partition Technique*, IEEE Access, vol. 5, pp. 27297–27310 (2017).

[17] Tripathi S.M., Tiwari A.N., Singh D., *Optimum design of proportional-integral controllers in grid-integrated PMSG-based wind energy conversion system*, International Transactions on Electrical Energy Systems, vol. 26, no. 5, pp. 1006–1031 (2016).

[18] Tahri A., Hassaine S., Moreau S., *A robust control for permanent magnet synchronous generator associated with variable speed wind turbine*, Journal of Electrical Engineering, vol. 15, no. 2, pp. 1–8 (2015).

[19] Raisemche A., Boukhnifer M., Larouci C., Diallo D., *Two active fault-tolerant control schemes of induction-motor drive in EV or HEV*, IEEE Transactions on Vehicular Technology, vol. 63, no. 1, pp. 19–29 (2014).

[20] Rothenhagen K., Fuchs F.W., *Current sensor fault detection, identification, and reconfiguration for doubly fed induction generators*, Proceeding of Industrial Electronics Society33rd Annual Conference of the IEEE, Taipei, Taiwan, pp. 1115–1120 (2007).

[21] Chi S., Xu L., Zhang Z., *Sliding mode sensorless control of PM synchronous motor for direct-driven washing machines*, Proceeding of Industry Applications Conference 41st IAS Annual Meeting Conference Record of the 2006 IEEE, Tampa, FL, USA, pp. 873–879 (2006).